

Outline of climate and oceanic conditions in the Indian Ocean: an update to mid-2018

Francis MARSAC¹ & Hervé DEMARCQ²
 IRD
 UMR 248 MARBEC
 Sète, France

Abstract

The trend and variability of climate and oceanic variables were investigated with emphasis on the conditions for the recent years (2016-2018). The ENSO cycle has been mostly in a neutral phase since September 2016, however a La Niña event developed between October 2017 and March 2018. Normal conditions prevailed since then but there is a high probability (65-70%) that an El Niño develops by the end of 2018. The Indian Ocean Dipole was in negative phase in 2017 and turned into a positive phase in 2017. There is a high probability that it returns to a normal phase by December. These cycles were associated to inter-annual changes in SST, thermocline depth and sea surface chlorophyll. However, in 2017, the thermocline pattern did not exhibit the typical situation observed during a positive dipole as the mixed layer remained shallow throughout 2017 and until March 2018 between latitudes 10°N-10°S. These conditions which occurred in the core of the purse seine fishing grounds, could have promoted the vulnerability of schools to the purse seine gear. The recent trend (since 2014) in chlorophyll concentration is characterized by higher productivity which may promote the aggregation of tuna preys and ultimately, a greater abundance of tuna schools. That link between chlorophyll and CPUE on free schools and floating objects associated schools was further investigated. It leads to the conclusion that the chlorophyll concentration is an important factor to incorporate in CPUE standardization, in addition to other physical-derived factors.

1- Introduction

Several descriptors of the ocean status are examined to depict the inter-annual variability and to track major changes that may have affected the large pelagic ecosystem in the recent years. To some extent, the environmental descriptors form a complementary set of information that can be useful to inform the WPTT for the stock management advice.

2- Data sources

Various sources of data are used in this paper:

- climate indices based on (i) sea level pressure anomalies, such as the Southern Oscillation Index (SOI) that depicts the ENSO cycle, the Indian Oscillation Index (IOI, Marsac and Le Blanc, 1998); and (ii) a sea surface temperature-derived index, the Dipole Mode Index (DMI, Saji et al, 1999) reflecting a mode of variability that is specific to the Indian Ocean (and coupled to some extent to the ENSO).
- the chlorophyll-a concentration from SeaWifs (1997-2002) and Modis (2003-present) satellite-mounted sensors, giving an index of ocean surface productivity (enhancement or depletion).
- sea surface temperature (SST) from the ERSSTv4 dataset (Huang et al, 2015), a monthly product at a 2° grid resolution. This dataset is used to compute the DMI.

¹ Email : francis.marsac@ird.fr

² Email : herve.demarcq@ird.fr

- sea surface temperature from the OISSTv2 dataset (*NOAA_OI_SST_V2 data provided by the NOAA/OAR/ESRL PSD, Boulder, Colorado, USA, <https://www.esrl.noaa.gov/psd/>*) a product at a 1°grid/month resolution used in this paper for maps (Reynolds et al, 2002).
- the NOAA/NCEP Global Ocean Data Assimilation System (GODAS) which provides monthly fields of temperature, salinity, vertical velocity and current for 40 depth levels (5 to 4500 m), along a 1° longitude/0.33° latitude grid globally. We derived the depth of thermocline by interpolating the depth of the 20°C between consecutive temperature at depths in the upper 300m of the water column.

More details on the datasets and methods used to produce the variables can be found in Marsac (2013). All data have been updated to July or September 2018 (depending on the datasets).

3- Variability and trends in the oceanic environment

Climate indices

The SOI indicates that the last El Niño event (positive phase of the ENSO cycle) occurred from March 2015 to April 2016 (Fig. 1a). The conditions returned to normal until September 2016, then shifted to a weak La Niña event until the turn of the year 2016-2017. ENSO was in a neutral phase from January to October 2017, then another La Niña event of greater magnitude occurred until March 2018. Since then, ENSO has returned to a neutral phase.

An ensemble analysis of multiple models predicts a 50-55% chance that an El Niño develops in September-November 2018, and a 65-70% chance that it would increase through the Northern Winter 2018-2019, which is triple the normal likelihood (NOAA, 2018).

The IOI was dominated by negative values (reflecting low pressure anomalies and warm conditions in the West IO) since 2007. Then positive anomalies developed through the second semester of 2016 and first quarter of 2017. The IOI has returned to a neutral phase since mid-2017 (Fig. 1b)

The DMI went through 3 significant positive phases in the years 2000s: 2007 (coincident to an El Niño event), 2012 and 2017, so barely a 5-year oscillation. Negative dipoles were less marked than positive dipoles, and were observed in 2005, 2010 and 2016 (Fig. 2). Four of the six international climate models surveyed by the Australian Bureau of Meteorology suggest that index values will remain above positive IOD thresholds for the remainder of October 2018. All models expect a return to neutral by December and through the first quarter 2019. A focus on the SST anomalies in the WIO, EIO and the DMI for the 5 past years is shown in Fig. 3.

All three indices are significantly correlated, with the highest correlation found between IOI and SOI ($r_s = +0.46$, $p < .001$). With respect to DMI, the highest correlation is found with IOI ($r_s = -0.23$, $p < 0.001$) compared to that with SOI ($r_s = -0.15$, $p < 0.001$) which makes sense as DMI and IOI include a mode of variability which is specific to the Indian Ocean.

Main oceanic features over 2016-2018 (Fig. 4a-f)

- During the first quarter 2016 (January-April), the striking feature was a deep thermocline structure between 5°S-10°S (in the equatorial counter-current). The core of that structure exhibited a deepening of 40-60m compared to normal, and propagated westwards from 60-72°E in January to 50°E-60°E in April.
- During the following austral winter (June-September 2016), the SST was colder than normal (-1°C to -1.5°C) in the Somali basin, reflecting an active upwelling that year. Shallow mixed layer (-30 to -40m) developed off Somalia from June to August 2016 and along a latitudinal belt ranging from 2°S to 10°S, 50°E to 100°E. Hot spots of sea surface chlorophyll (SSC) were observed in association with cool SST patches and shallow mixed layer, mostly in the WIO.
- In the East Indian Ocean (EIO; 90°E-110°E), a deep mixed layer started to develop in July 2016, gradually reaching its climax in September 2016 (+40m). The anomaly remained

noticeable until January 2017. Associated to that deepening, SSC remained in a depleted phase off Sumatra.

- Hot spots of SSC (+0.3 to +0.4 mg/m³) were observed from September to December 2016 along the West coast of India, the Lakshadweep, the Maldives and Sri Lanka.
- SST was normal from October 2016 to April 2017 in most of the WIO (10°N to 20°S) except a ridge of cool anomalies in January 2017 between 10°S and 20°S. Thermocline shoaled of about 20 to 50m over most of the WIO from January to April 2017. Few hotspots of high SSC were observed during that period, whereas low SSC was observed along the Somalian coast from December 2016 to February 2017. However most of the WIO was under normal SSC until April 2017.
- A positive Indian Ocean Dipole started to develop in May 2017, with positive SST anomalies (+0.5 to +1.0°C) observed in the WIO from May to September 2017. At the same time, cold anomalies occurred in the EIO, between Java and Australia. However, the thermocline pattern did not exhibit the typical situation observed during a positive dipole as the mixed layer remained shallow throughout 2017 and until March 2018 between latitudes 10°N-10°S.
- During 2018, SST varied between above- and below-normal anomalies throughout the IO. A clear positive dipole pattern started to develop in September 2018, with warm anomalies [+1.0 to +1.5°C] in the WIO and cold anomalies [-0.5 to -1.5°C] in the EIO.
- Deep mixed layer was observed in the South central IO in April 2018, and spread gradually to the north (to 5°S) until the last month with available observations (August 2018). Very shallow thermocline was observed during the Somali upwelling season in the Arabian Sea.
- The SSC was high along Somalia in January 2018, and in the Arabian Sea from January to March 2018. The SSC was again higher than normal off Somalia at the onset of the upwelling (June) and through July and August (the last month with observations).

Regional analyses

The yearly trend in chlorophyll concentration for 5 sub-areas distinguishes three groups with similar patterns (Fig.5 and 6):

- Somali basin (SOM) and Mozambique Channel (MOZ) are the most productive areas (0.30 to 0.54 mg.m⁻³), as a consequence of the seasonal upwelling along the Somalian coast and the intense mesoscale activity in the Mozambique Channel. The SSC has steadily increased in SOM region and peaked in 2017. The value for 2018 in SOM is probably underestimated as it does not include the full upwelling season where SSC is enhanced. The bias of missing values for the second semester 2018 in MOZ is likely to be minor because the highest productive season is February-July that is already included in the current SSC estimate. SSC estimates for 2017 in both areas belong to the 3rd quartile of the distribution of the whole yearly series.
- West equatorial zone (WEQ) and Maldives (MAL) display intermediate values (0.11 to 0.22 mg.m⁻³) and have followed a similar trends since 2005. In 2017 the chlorophyll content continued to increase in MAL whereas it remained similar to 2016 in WEQ. SSC estimates for 2017 in both areas belong to the 3rd quartile of the distribution of the whole yearly series.
- The East tropical region (ETR) is less productive than the former groups, with values ranging from 0.08 to 0.12 mg.m⁻³. The SSC peaked in the years 1999, 2011 and 2017. The chlorophyll concentration has steadily increased since 2014. The SSC estimate for 2017, located in the 4th quartile of the yearly distribution, is the second largest in the series (after 1999).

The overall rate of change is defined as the increase or decrease in % from the average 1998-2017. For 2016 and 2017, the rate is based on the annual average for the series, whereas it is based on the January-July average for 2018 to account for the incompleteness of observations for that year (Table 1). For all three years, the primary productivity is above the 20-year average for most of the regions. Positive rates are particularly high in 2017 (up to +16.4% in the ETR). SOM and WEQ are the two zones with consecutive above-normal SSC. These estimates indicate a phase of higher than normal

productivity in the IO, with potentially better foraging conditions for intermediate and high trophic levels.

The seasonal SST, 20°C isothermal depth and surface chlorophyll concentration for each of the 5 sub-areas, 1998-2017, are shown in Figs 7 to 11.

Table 1 – Rate of change (in %) of surface chlorophyll concentration

	SOM	MAL	WEQ	ETR	MOZ
2016	+2.1	+1.4	+8.3	-2.7	+4.8
2017	+8.9	+9.0	+6.1	+16.4	+0.1
2018 (Jan-Jul)	+7.3	-4.1	+21.5	+3.2	-1.8

4- Links between surface chlorophyll content and yellowfin CPUE

In this section, we investigate the link between the chlorophyll concentration and the standardized yellowfin CPUE computed from the European purse seine fleets (Katara et al, 2018). This analysis distinguishes the free schools (FS) sets and the floating object-associated (FOB) sets. The former is intended to reflect abundance of large individuals (mostly spawners) whereas the latter would reflect the abundance of juvenile fish. The purse seine standardized CPUE (Katara et al, 2018) calculated for 1986-2017 includes a variety of variables, including environmental variables such as thermocline depth and vertical current shear. Initially, it was intended to include the chlorophyll concentration, however additional models had to be run on a shorter time period as sea colour measurements only started in 1997 with SeaWifs. Due to time constraints, it was not possible to perform these additional runs. Therefore, we analyse here the relationship of the standardized CPUE for both FSC (1997-2017) and FOB (2007-2017).

As the final CPUE indices are not spatialized, we had to select an area from where a chlorophyll index could be derived, provided that it should be geographically connected to the PS fishery area. We used the result of a principal component analysis (Empirical Orthogonal Function-EOF) on chlorophyll concentration performed in 2012 (Marsac, 2012). The spatial pattern of variability of the 1st EOF (highlight the Somali Basin as a hot spot area catching most of the inter-annual variability (Fig 12). The chlorophyll index used in this analysis is the log-transformed monthly average over the hot spot area, between 10°N-5°S and 40°E-60°E.

Free schools sets

The model used to standardize catch per hour on free schools was split in 2 components: a binomial model to establish the probability of making a positive set, and a lognormal model to analyse the catch per hour conditional to YFT catch > 0. The final model (delta lognormal) was the product of the 2 components (Katara et al, 2018).

We performed GAMs to analyse the relationships of each of the component and the final model with the log-transformed chlorophyll concentration. The largest percentage of deviance explained was obtained for the probability of making a positive set. The shape of the curve suggests that the probability (logit) increases with chlorophyll concentration until it reaches a given threshold (-1.3, i.e. 0.27 mg/m³) above which it forms a plateau (Fig. 13). The % of deviance of the GAM using the lognormal CPUE is 5.6% and the shape of the relationship is a plateau followed by an increasing slope about the same thresholds as previously (Fig 14). A GLM was performed with the Chlorophyll/probability (logit) case only. The output plots are presented in Fig. 15. The residuals are slightly skewed and there also is a slight trend in the residuals. However Chlorophyll is highly significant at the level $p < 0.001$.

Floating-object associated sets

The model used to standardize catch per positive set was a lognormal model only, as the ratio of positive sets remains high (90%) and stable (Katara et al, 2018). A GAM was performed with the log-transformed chlorophyll concentration for the full year and explained 13.1% of the deviance (Fig. 16). Considering that chlorophyll is enhanced in the region during the upwelling (June to September), a GAM was run on this restricted period of time for chlorophyll and CPUE, and the deviance explained was 43% (Fig. 17). However, a small number of observations for that period (n=44) has to be noted, which is questionable for GAMs. We then did a GLM for the restricted period. The fit is quite good, the residuals are quasi-normally distributed and there is no trend in the residuals over the predicted values (Fig. 18).

Discussion

The results show that the probability of making a positive set on free schools increases with the chlorophyll concentration. The decision for a skipper to set a free school depends highly on the size and the density of the school. Scattered fish and schools are difficult to set and the skipper will often wait that schools gather in a single and large one to make a set, if this occurs. The high chlorophyll content indicates a great potential for the concentration of prey species, and ultimately, tuna would congregate for frenzy feeding by forming dense schools. This might explain the link between the chlorophyll concentration and the probability of making a positive set. That link is much weaker for the amount of catch per hour conditional to positive catch, as many other factors interplay in the success of a set.

As for FOB-associated sets, the link is strong with chlorophyll especially during the upwelling season (June-September). The upwelling generates a high primary production which is carried away towards the Somalian gyre, and intermediate trophic levels develop during that transport. Numerous FOBs are trapped in the Somalian gyre during that season, then the aggregative behaviour may be strengthened by favourable foraging conditions. As just-recruited tunas are found at FOBs during that season, it could be assumed that years with intense upwelling will increase growth and potentially abundance of such juvenile tunas.

5- Conclusion

The environmental conditions in the IO have fluctuated according the Indian Ocean Dipole and the most recent event was recorded in 2017. Fluctuations are well reflected in the sea surface temperature, the depth of the mixed layer and the surface chlorophyll. The mixed layer remained shallow throughout 2017 and until March 2018 between latitudes 10°N-10°S. These conditions which occurred in the core of the purse seine fishing grounds, could have promoted the vulnerability of schools to the purse seine gear. The recent trend (since 2014) in chlorophyll concentration is characterized by higher productivity which may promote the aggregation of tuna preys and ultimately, a greater abundance of tuna schools.

Katara et al (2018) show in their models the effect of environmental factors on CPUE standardization, especially the depth of the thermocline. Because of time constraint, they could not run models incorporating the chlorophyll concentration. This analysis suggests that the incorporation of a chlorophyll index would be valuable in purse seine CPUE standardization, and this should be recommended for future assessments.

Acknowledgements

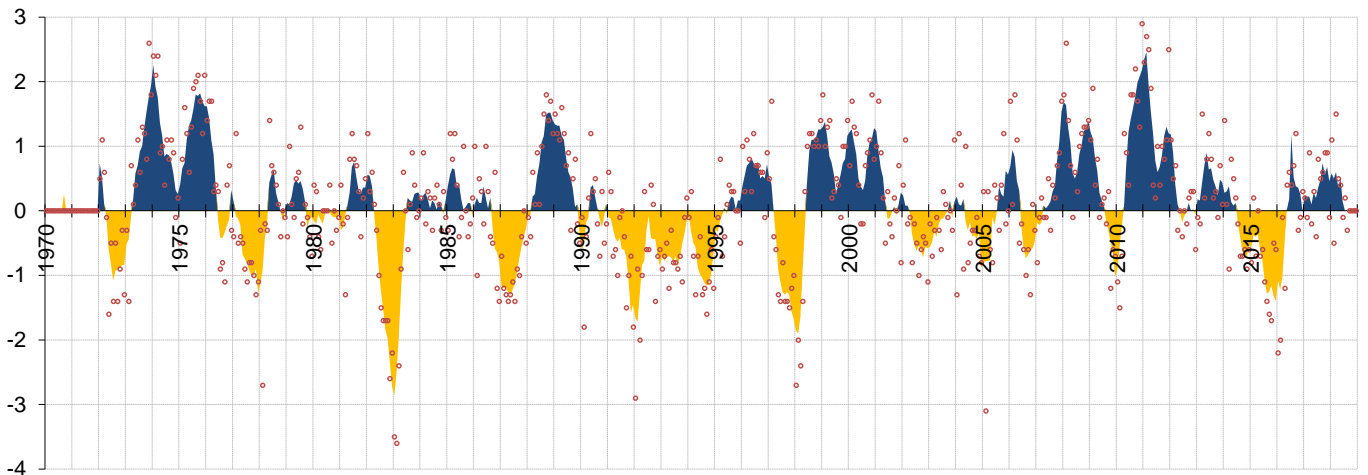
We are grateful to the Climate Centre of the Seychelles National Meteorological Services, and particularly to Marcel Belmont, a senior technician of this Centre, for the provision of sea level pressure data used to compute the IOI.

References

- Bureau of Meteorology, Australia (2018). Indian Ocean Dipole outlooks. <http://www.bom.gov.au/climate/enso/#tabs=Indian-Ocean>
- Huang, B., Banzon, V.F., Freeman, E., Lawrimore, J., Liu, W., Peterson, T.C., Smith, T.M., Thorne, P.W., Woodruff, S.D. and Zhang, H.-M. (2015). Extended Reconstructed Sea Surface Temperature version 4 (ERSST.v4): Part I. Upgrades and intercomparisons. *J. Climate*, doi:10.1175/JCLI-D-14-00006.1
- Katara, I., Gaertner, D., Marsac, F., Grande, M., Kaplan, D., Urtizberea, A., Guery, L., Depetris, M., Duparc, A., Floch, L., Lopez, J. and Abascal, F. (2018). Standardization of yellowfin tuna CPUE for the EU purse seine fleet operating in the Indian Ocean. *20th session of the Working Party on Tropical Tuna*. IOTC-2018-WPTT20-36, 14 p
- Marsac, F. (2012). Outline of climate and oceanographic conditions in the Indian Ocean over the period 2002-2012. *14th Session of the Working Party on Tropical Tuna*. IOTC-2012-WPTT14-09, 16 p.
- Marsac, F. (2013). Outline of climate and oceanographic conditions in the Indian Ocean: an update to August 2013. *15th Session of the Working Party on Tropical Tuna*. IOTC-2013-WPTT15-09, 14 p.
- Marsac, F., Le Blanc, J-L. (1998). Interannual and ENSO-associated variability of the coupled ocean-atmosphere system with possible impacts on the yellowfin tuna fisheries of the Indian and Atlantic oceans. In: J.S. Beckett (Ed). *ICCAT Tuna Symposium. Coll. Vol. Sci. Pap.*, L(1) : 345-377.
- NOAA, 2018. Climate Diagnostics Bulletin August 2018. Near real-time ocean/atmosphere, monitoring, assessment and prediction. 89 p.
- Reynolds, R.W., Rayner, N.A., Smith, T.M., Stokes, D.C., and Wang, W. (2002): An improved in situ and satellite SST analysis for climate. *J. Climate*, 15, 1609-1625
- Saji, N.H., Goswami, B.N., Vinayachandran, P.N., Yamagata, T. (1999). A dipole mode in the tropical Indian Ocean. *Nature* 401: 360-363
-

(a)

Southern Oscillation Index



(b)

Indian Oscillation Index

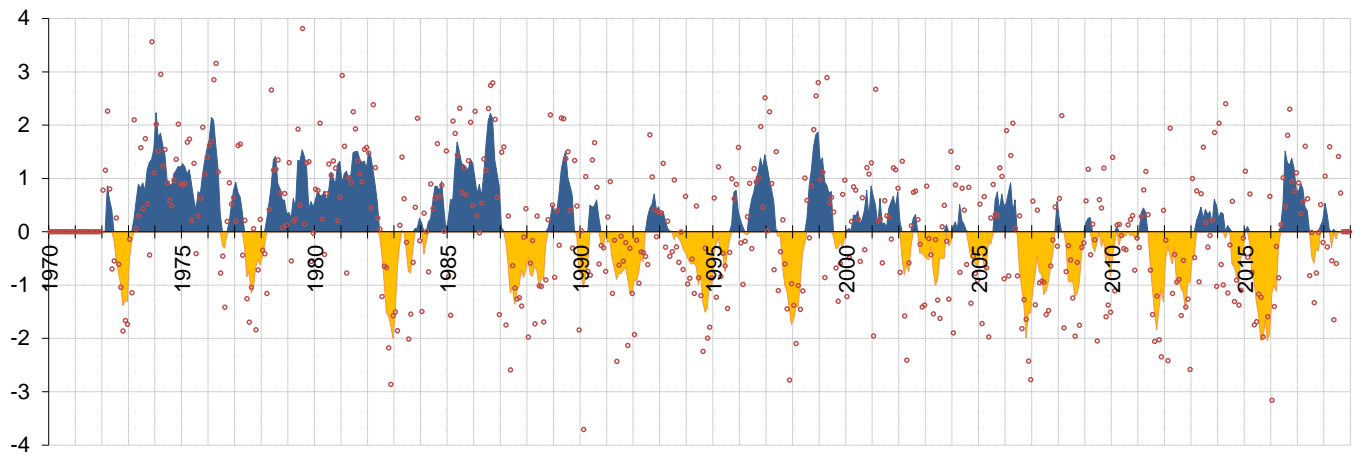


Fig.1 – (a) The Southern Oscillation Index (SOI) and (b) the Indian Oscillation Index (IOI), January 1970 to August 2018. The color shaded area represents the 5-month moving average, whereas observed monthly values are shown in red dots. El Niño events correspond to the extreme negative values whereas La Niña events are described by the extreme positive values of the SOI.

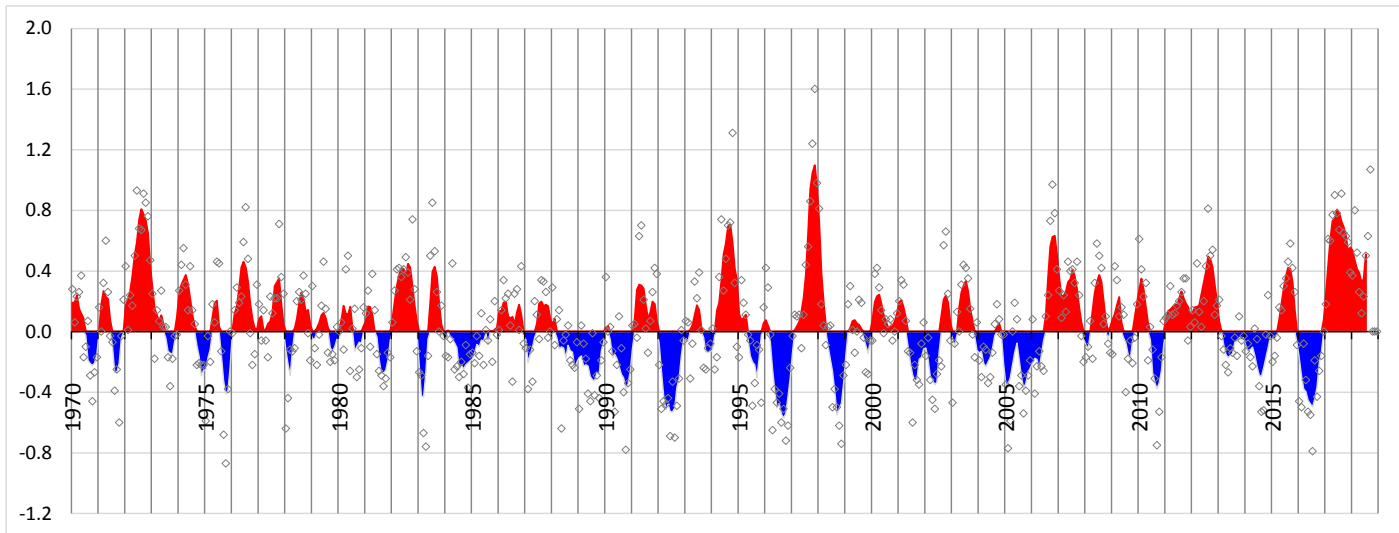


Fig.2 - Dipole mode, January 1970 – September 2018. The shaded area of IOI is a 5-months moving average whereas observed monthly values are represented in black empty dots. The DMI series is 5-month moving average. For a given anomaly, IOI and DMI are opposite sign.

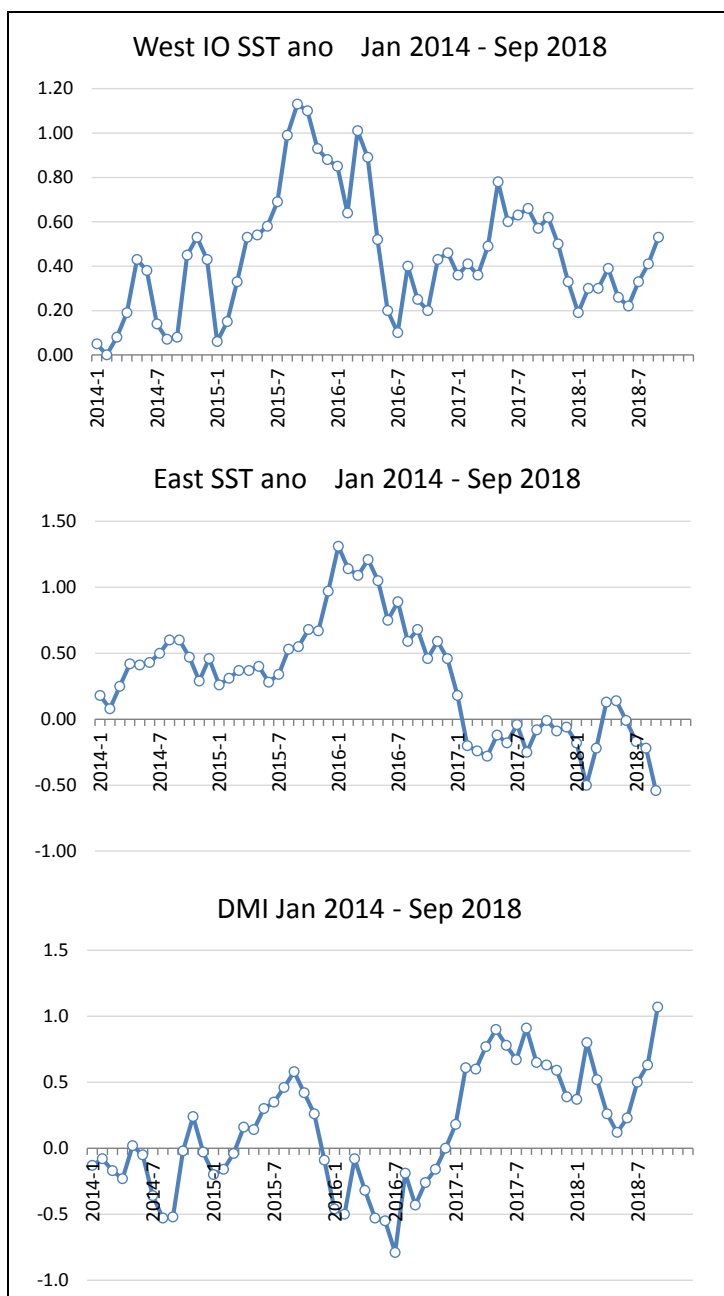


Fig.3 -Non-smoothed SST anomalies in the West IO (top), East IOI (middle) and DMI (bottom) for January 2014-September 2018

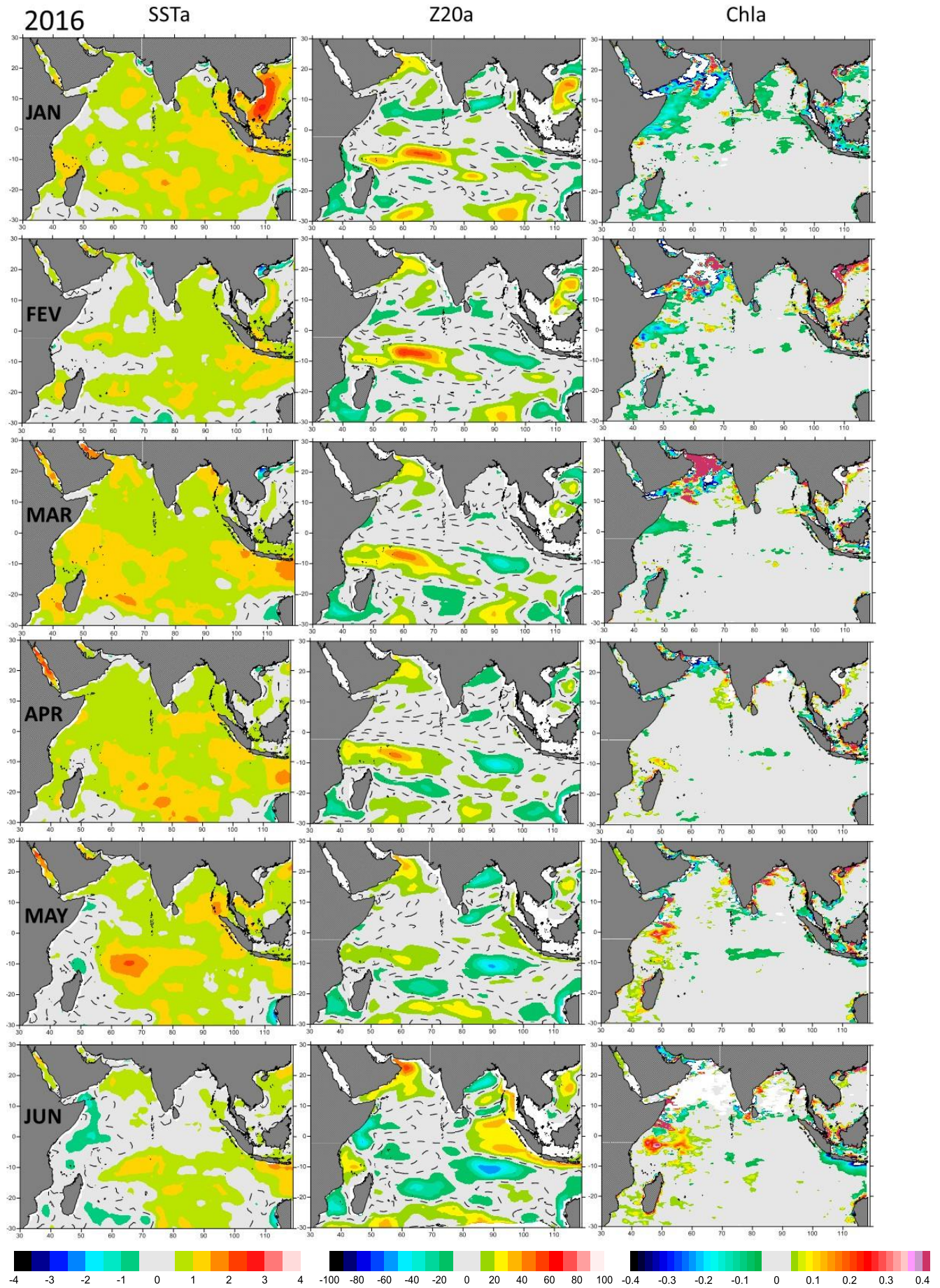


Fig. 4a – Geographic distribution of anomalies for sea surface temperature (°C, left), 20°C isothermal depth (m, middle) and sea surface chlorophyll (mg.m^{-3} , right) for the first semester of 2016. Grey shading indicates minor anomalies about the mean. Thus, the more significant anomalies (colour shading) are displayed.

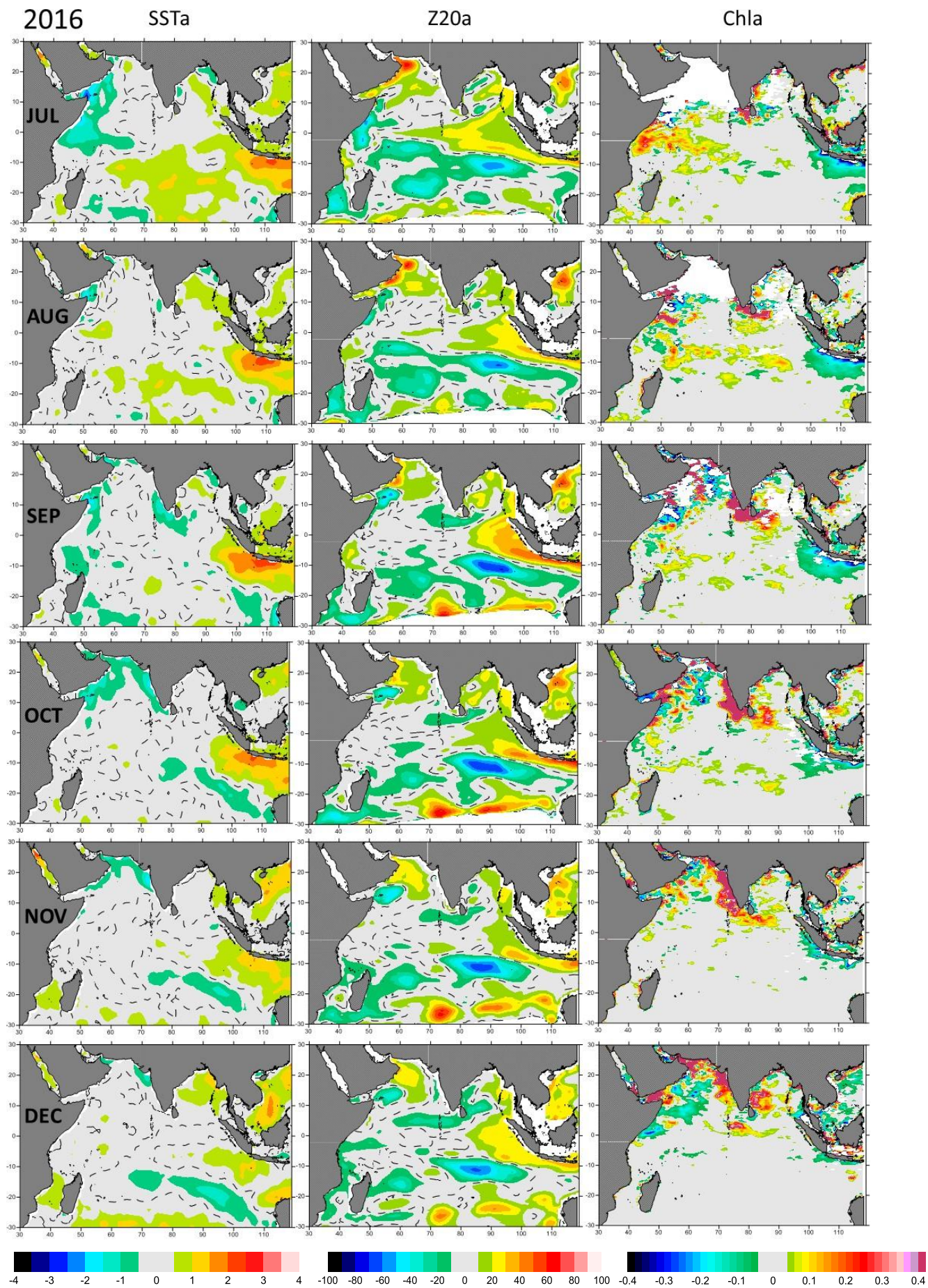


Fig. 4b – Same as above, for the second semester of 2016

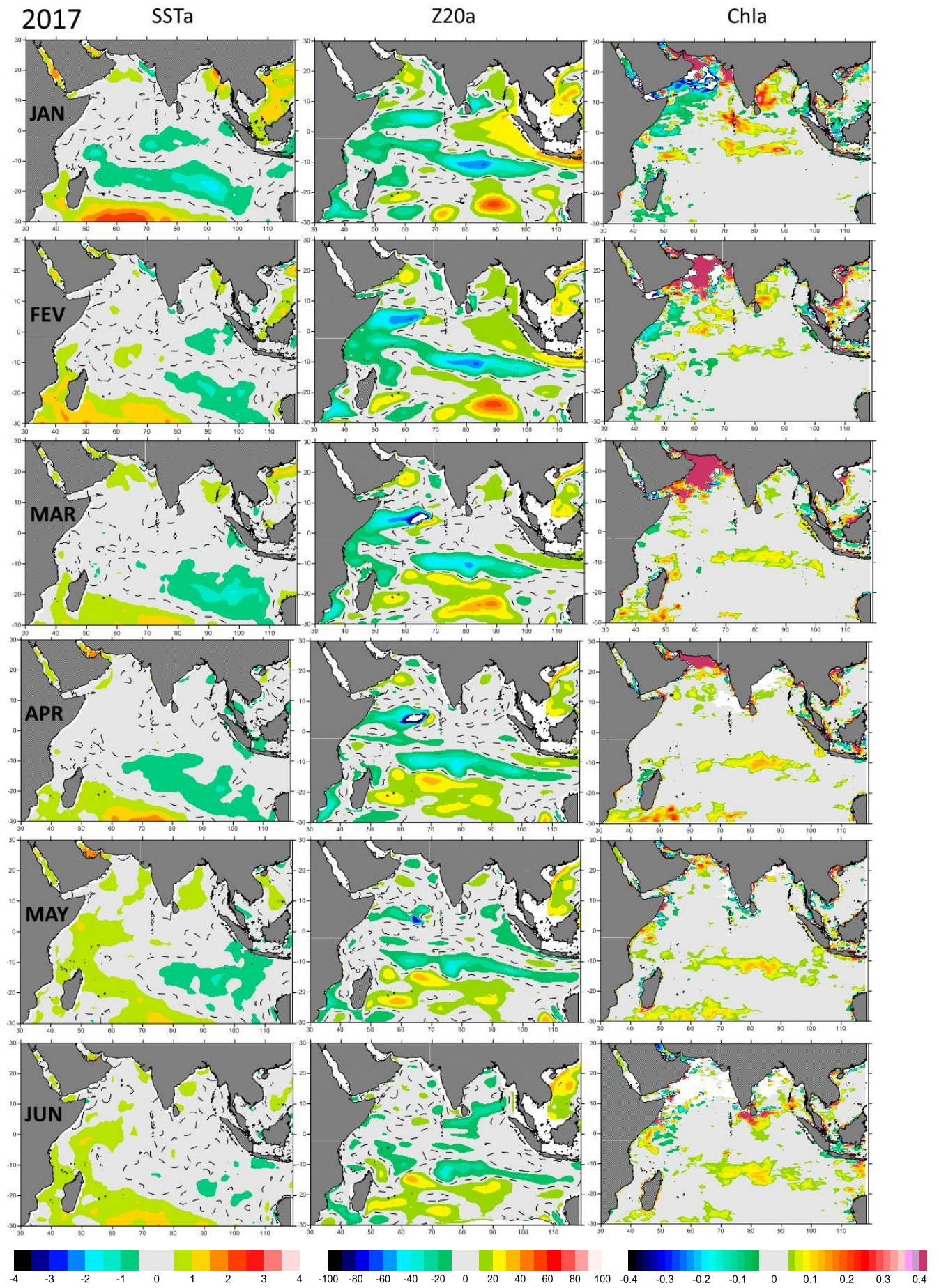


Fig. 4c – Same as above, for the first semester of 2017.

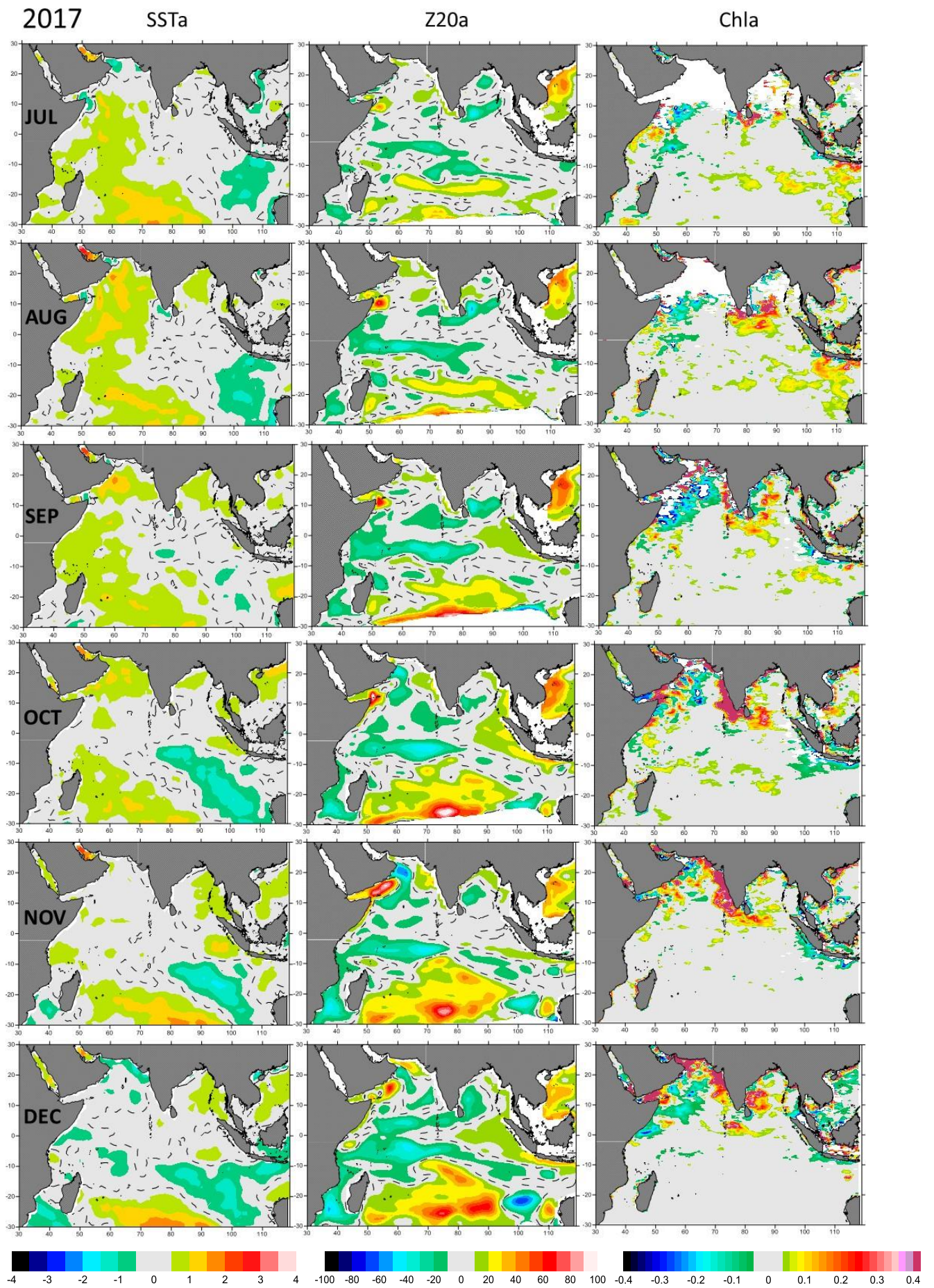


Fig. 4d – Same as above, for the second semester of 2017.

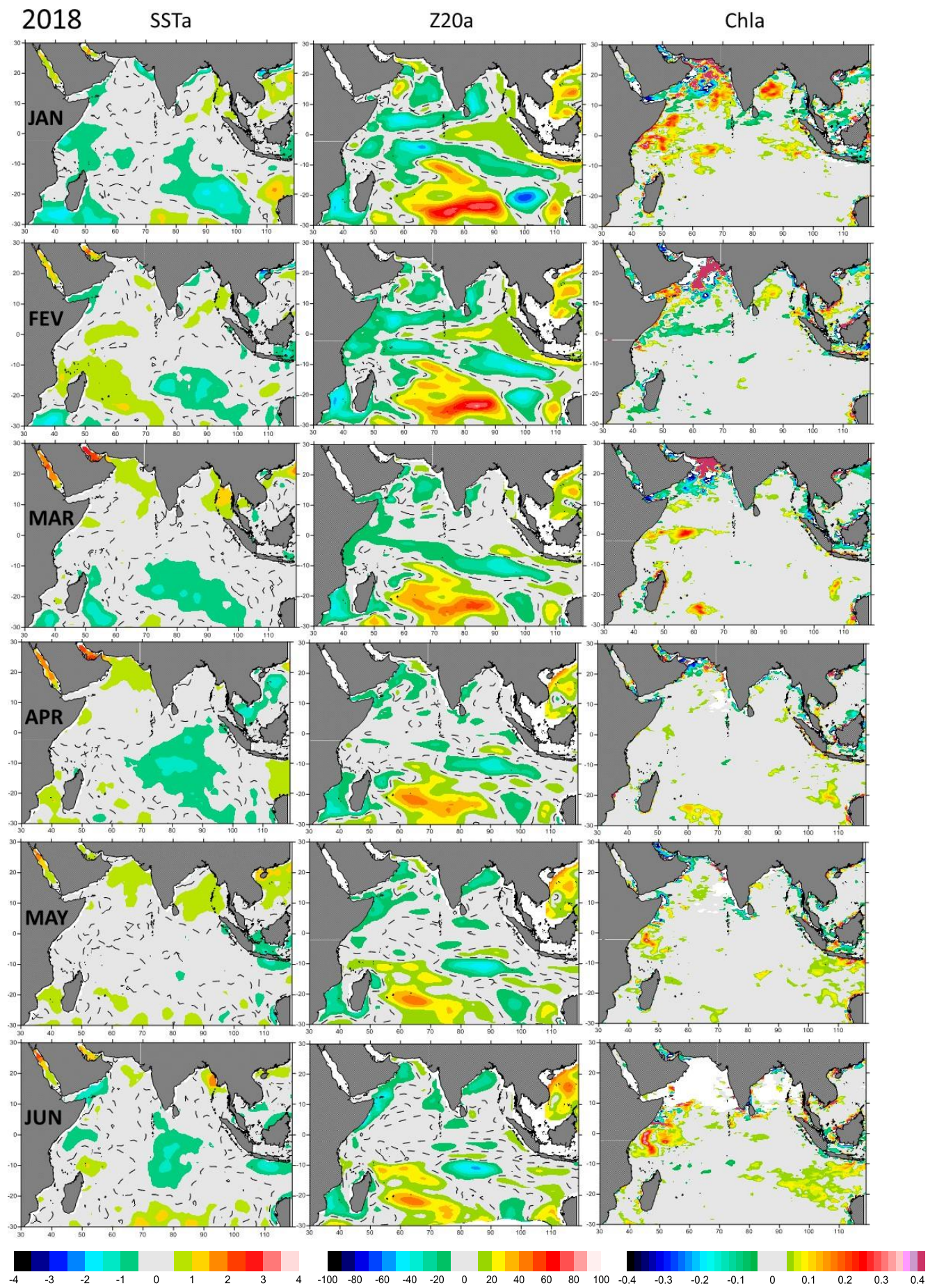


Fig. 4e – Same as above, for the first semester of 2018.

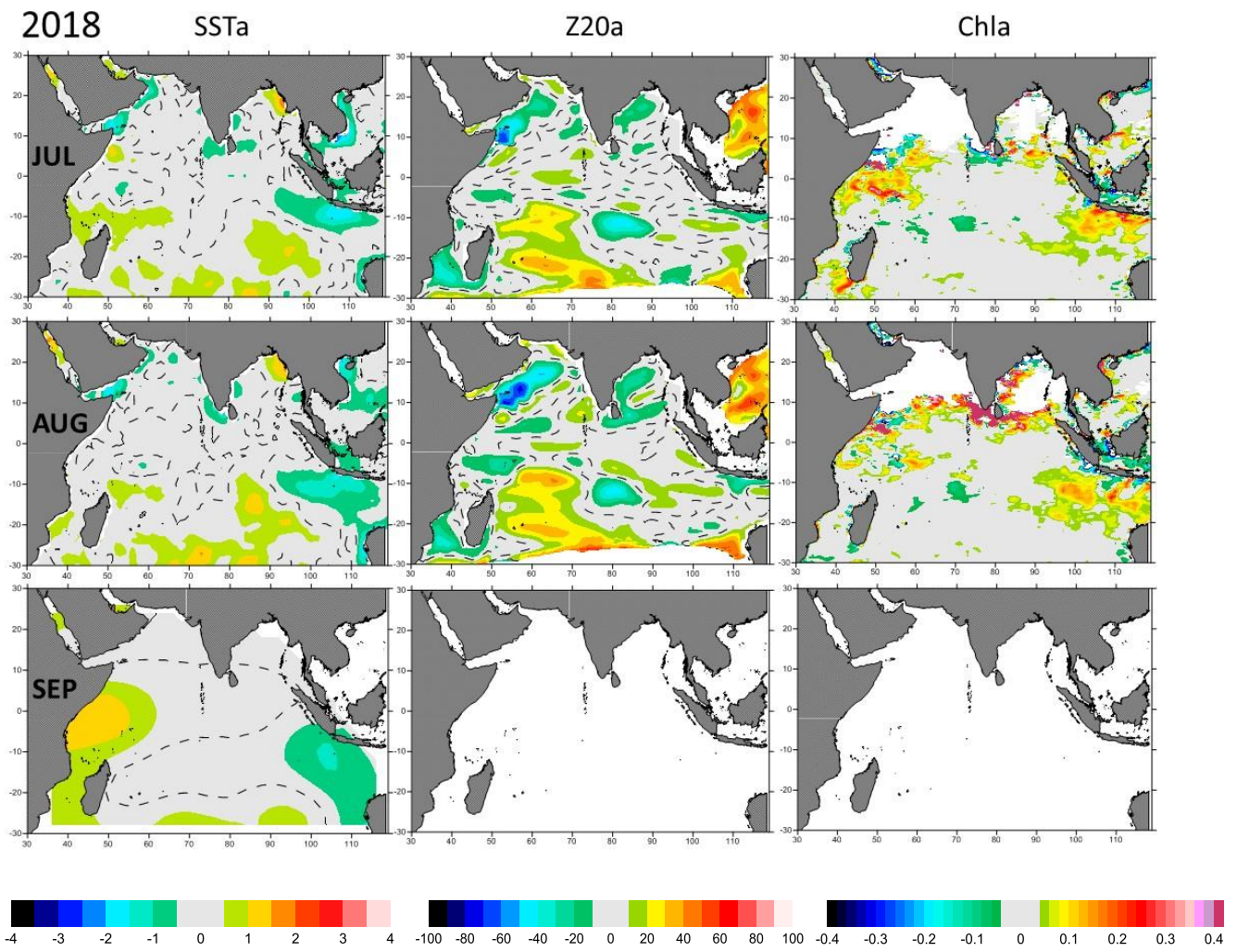


Fig. 4f – Same as above, for the 3rd quarter of 2018.

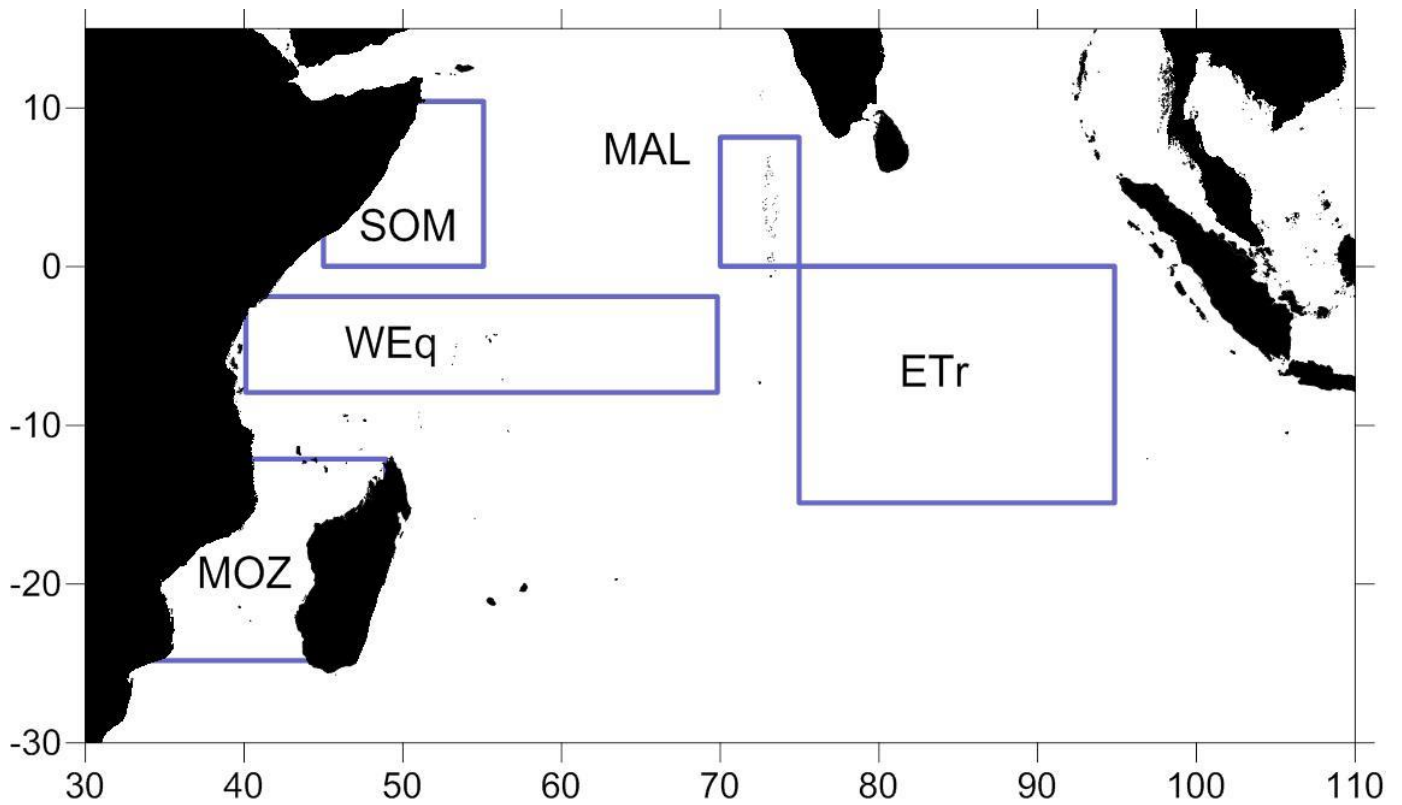


Fig. 5 - Area stratification used for the regional analysis.

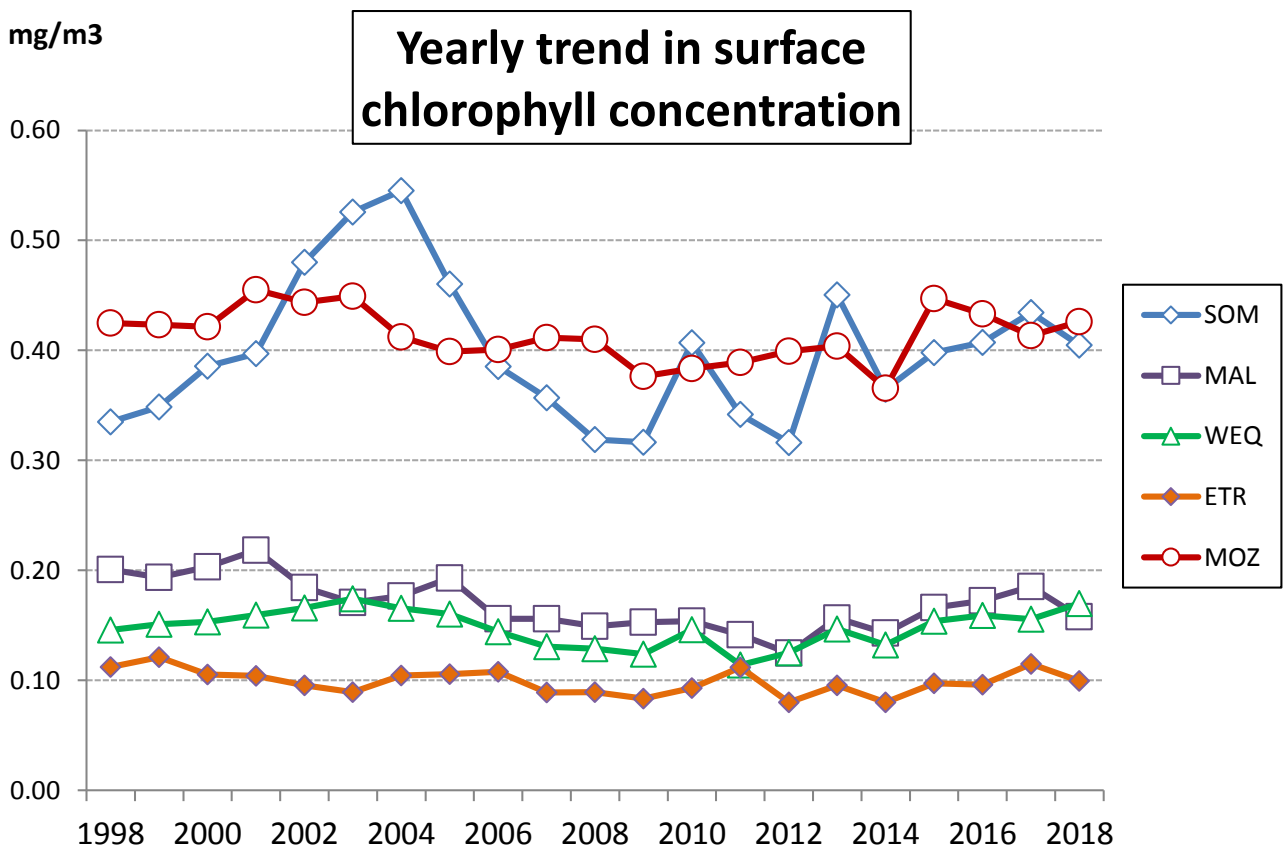


Fig.6 – Yearly trend of sea surface chlorophyll concentration measured by satellite, 1998-2018 (Seawifs 1998-2002 / Modis since 2003). Note that 2018 is incomplete (ends in August).

SOMALI BASIN

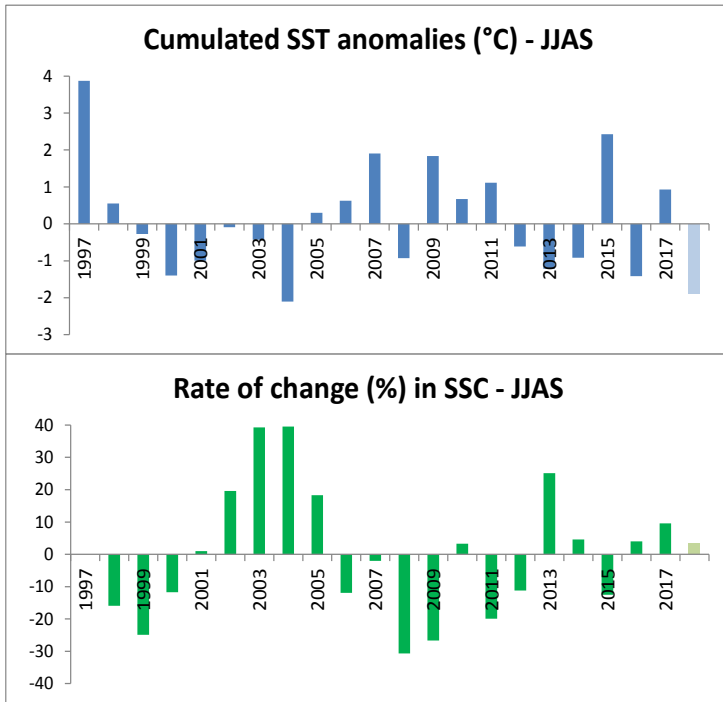


Fig. 7 – SST and surface chlorophyll (SSC) trends during the south-west monsoon, average June to September, in the Somalian basin. SST anomalies are cumulated over the season. Chlorophyll is expressed as rate of change about the 1998-2017 mean, June to September. The incomplete years are marked with light colour bars

MOZAMBIQUE CHANNEL

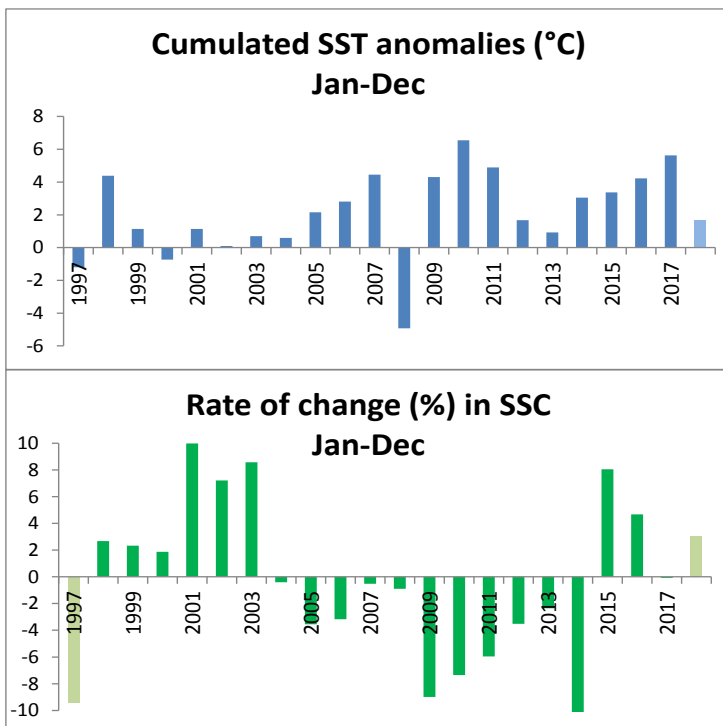


Fig. 8 – SST and surface chlorophyll (SSC) trends in the Mozambique Channel. SST anomalies are cumulated over the year and chlorophyll is expressed as rate of change about the 1998-2017 mean for the study period. The incomplete years are marked with light colour bars.

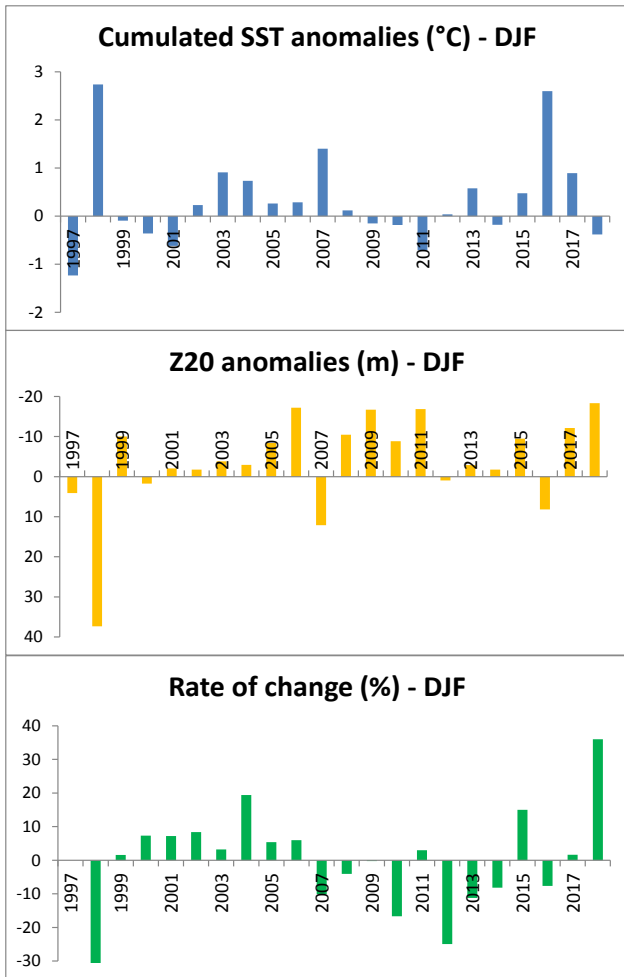


Fig. 9 – SST, 20°C isothermal depth and surface chlorophyll trends in the West Equatorial area, during the core of the north-east monsoon (December of year $y-1$ to February of year y). SST anomalies are cumulated over the season, Z20 anomalies are the mean over the season and chlorophyll is expressed as rate of change about the 1998-2018 average for the season. Negative (positive) Z20 anomalies denote shoaling (deepening) of the thermocline.

WEST EQUATORIAL AREA

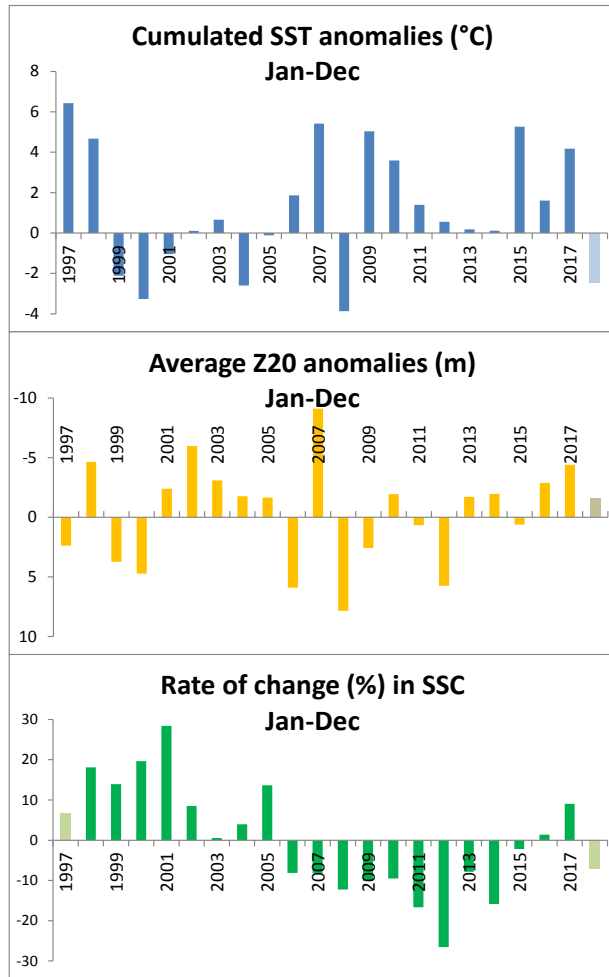
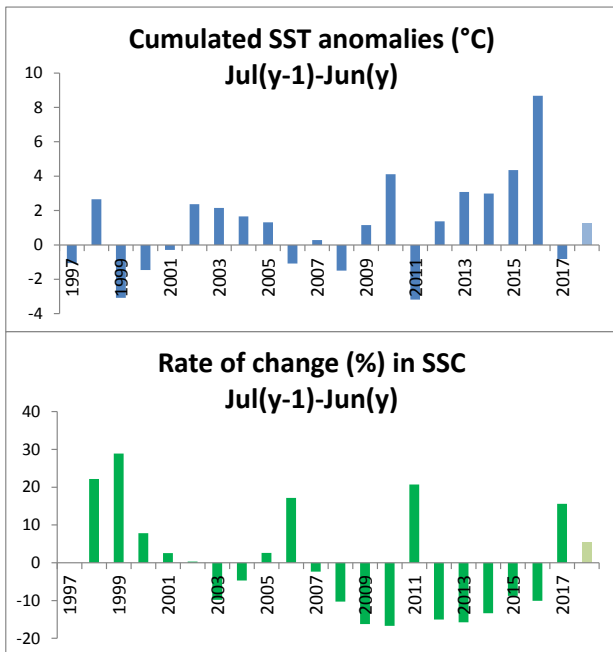


Fig. 10 – SST, 20°C isothermal depth and surface chlorophyll (SSC) trends in the Maldives. SST anomalies are cumulated over the year, Z20 anomalies are the average over the period and chlorophyll is expressed as rate of change about the 1998-2017 for the study period. Negative (positive) Z20 anomalies denote shoaling (deepening) of the thermocline. The incomplete years are marked with light colour bars

MALDIVES



EAST TROPICAL AREA

Fig. 11 – SST and chlorophyll (SSC) trends in the Eastern Tropical Indian Ocean, 12-month average from July (of the preceding year) to June (of the current year). SST anomalies are cumulated over the 12-month period and SSC is expressed as rate of change about the 1998-2017 for the same period. The incomplete years are marked with light colour bars

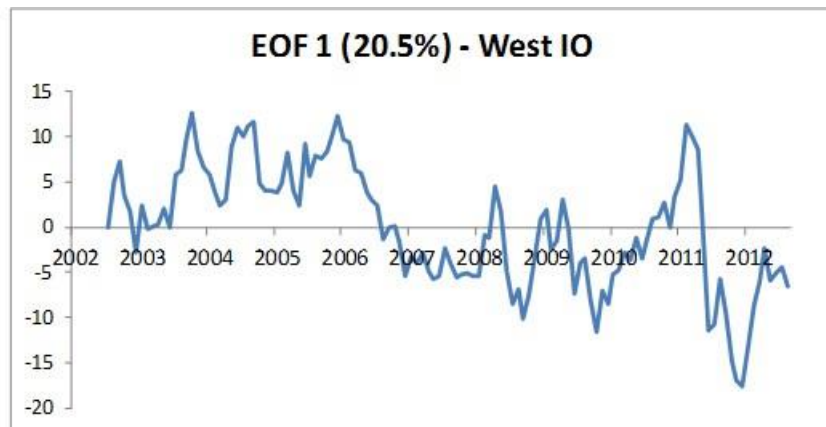
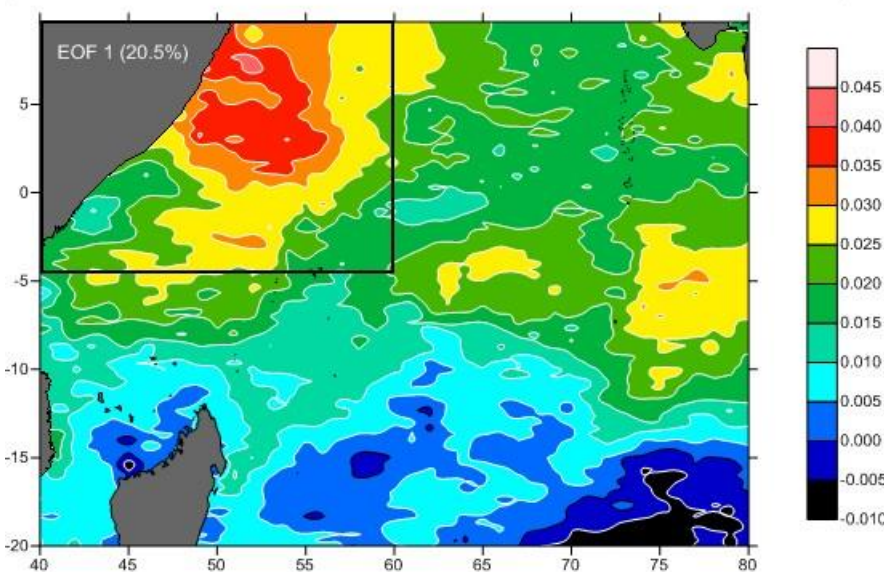


Fig. 12 - First EOF of the Sea Surface Chlorophyll in the West Indian Ocean. This EOF captures 20.5% of the variance. Top : temporal pattern; bottom: spatial pattern.

The temporal pattern shows a period of elevated chlorophyll concentration spanning from 2003 to 2006, followed by a phase dominated by negative anomalies from 2007 to 2012 (with the exception of 2011). The spatial pattern highlights the amount of variability in space. The Somali region is where the variability of the largest, towards enhancement or depletion, depending on the sign of the temporal coefficients. The box indicates the area where the chlorophyll index for this study is being calculated (from Marsac, 2012)



Formula: **proba** ~ s(logchl, bs = "cs")

Parametric coefficients:

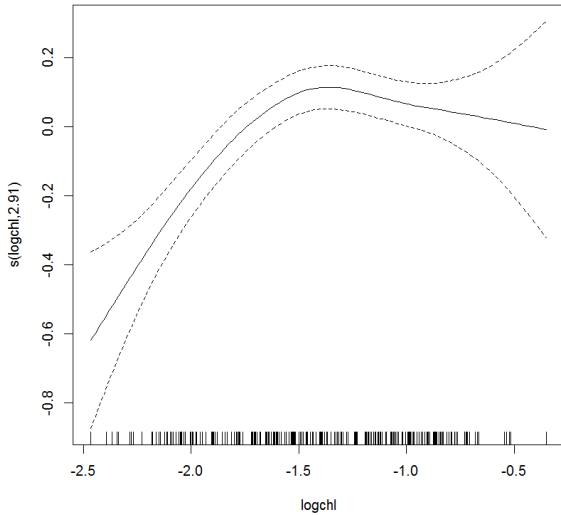
	Estimate	Std. Error	t value	Pr(> t)
(Intercept)	-0.85945	0.02539	-33.85	<2e-16 ***

Approximate significance of smooth terms:

	edf	Ref.df	F	p-value
s(logchl)	2.909	9	4.196	9.18e-09 ***

R-sq.(adj) = 0.136 Deviance explained = 14.7%
 GCV = 0.15793 Scale est. = 0.15537 n = 241

Fig. 13- GAM-derived effect of the chlorophyll concentration on the probability of making a positive set on free school



Formula: **lognormal** ~ s(logchl, bs = "cs")

Parametric coefficients:

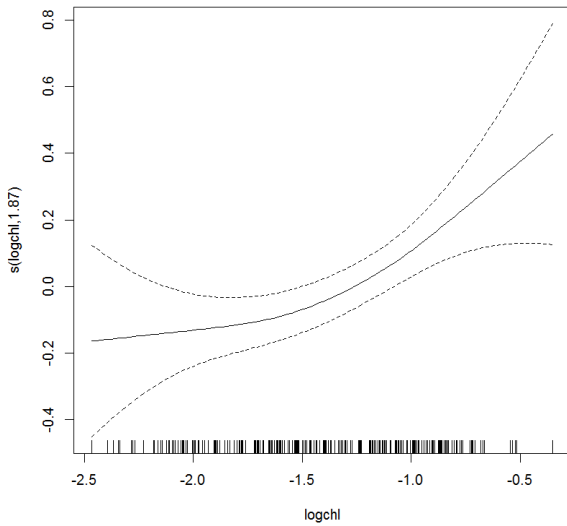
	Estimate	Std. Error	t value	Pr(> t)
(Intercept)	0.80548	0.03872	20.8	<2e-16 ***

Approximate significance of smooth terms:

	edf	Ref.df	F	p-value
s(logchl)	1.865	9	1.432	0.000663 ***

R-sq.(adj) = 0.0486 Deviance explained = 5.6%
 GCV = 0.36567 Scale est. = 0.36132 n = 241

Fig. 14 - GAM-derived effect of the chlorophyll concentration on the CPUE conditional to YFT catch > 0



glm(formula = **proba** ~ chloro, family = gaussian, data = TUNA_data)

Deviance Residuals:

Min	1Q	Median	3Q	Max
-1.06349	-0.30679	0.00826	0.27406	0.93214

Coefficients:

	Estimate	Std. Error	t value	Pr(> t)
(Intercept)	-0.16684	0.13038	-1.280	0.202
chloro	0.44593	0.08228	5.419	1.46e-07 ***

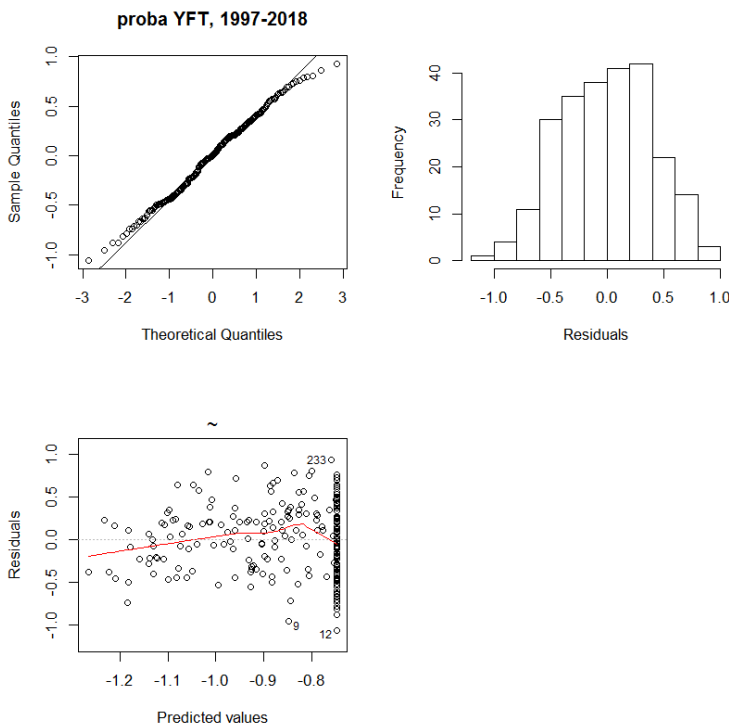
(Dispersion parameter for gaussian family taken to be 0.1608281)

Null deviance: 43.162 on 240 degrees of freedom

Residual deviance: 38.438 on 239 degrees of freedom

AIC: 247.51

Fig. 15 - Control plots of the GLM Chlorophyll / probability of making a positive set on free school



Formula: $\text{LogStdPUE} \sim s(\text{logchl}, \text{bs} = \text{"cs"})$

Parametric coefficients:

	Estimate	Std. Error	t value	Pr(> t)
(Intercept)	1.55965	0.02691	57.95	<2e-16 ***

Approximate significance of smooth terms:

	edf	Ref.df	F	p-value
s(logchl)	2.972	9	1.945	0.000338 ***

R-sq.(adj) = 0.111 Deviance explained = 13.1%
 GCV = 0.098564 Scale est = 0.095598 n = 132

Fig. 16 - GAM-derived effect of the chlorophyll concentration on the catch per positive set on FOB, all months of the year pooled

Formula: $\text{LogStdPUE} \sim s(\text{logchl}, \text{bs} = \text{"cs"})$

Parametric coefficients:

	Estimate	Std. Error	t value	Pr(> t)
(Intercept)	1.606	0.037	43.4	<2e-16 ***

Approximate significance of smooth terms:

	edf	Ref.df	F	p-value
s(logchl)	1.342	9	3.141	8.85e-07 ***

R-sq.(adj) = 0.412 Deviance explained = 43%
 GCV = 0.063619 Scale est. = 0.060232 n = 44

Fig. 17 - GAM-derived effect of the chlorophyll concentration on the catch per positive set on FOB, for June to September only.

$\text{glm}(\text{formula} = \text{LogStdPUE} \sim \text{logchl}, \text{family} = \text{gaussian}, \text{data} = \text{TUNA_data})$

Deviance Residuals:

Min	1Q	Median	3Q	Max
-0.52319	-0.18523	0.00077	0.15630	0.41791

Coefficients:

	Estimate	Std. Error	t value	Pr(> t)
(Intercept)	-2.6770	0.1935	13.83	< 2e-16
logchl	1.0821	0.1919	5.64	1.31e-06 ***

(Dispersion parameter for gaussian family taken to be 0.05964831)

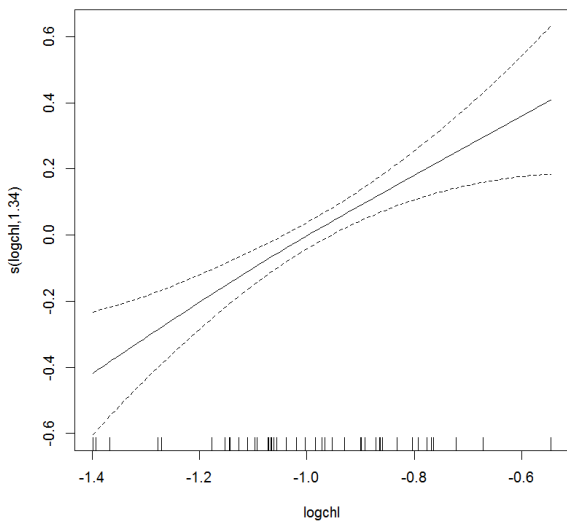
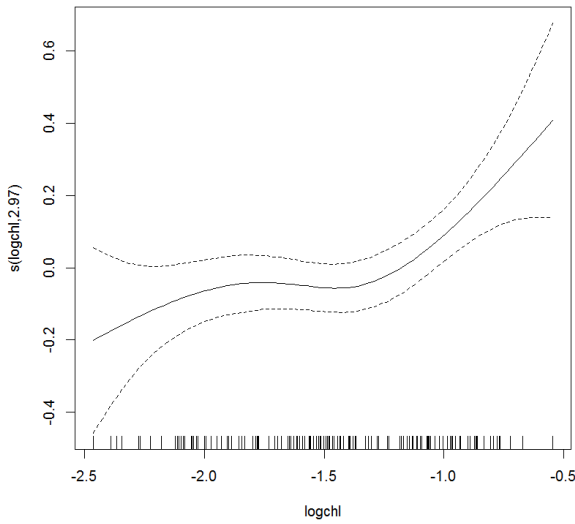
Null deviance: 4.4023 on 43 degrees of freedom

Residual deviance: 2.5052 on 42 degrees of freedom

AIC: 4.771

Fig. 18 - Control plots of the GLM

Chlorophyll/catch per positive set on FOB, June to September.



LogPUE FOB YFT Jun-Sep 2007-2018

